LETTER

Variance properties of the microwave absorption spectrum of an ensemble of nitrogen vacancy centers in diamond

To cite this article: R. A. Chelly *et al* 2023 *EPL* **144** 56002

A Letters Journal Exploring the Frontiers of Physics

December 2023

EPL, **144** (2023) 56002
doi: 10.1209/0295-5075/ad116d

www.epljournal.org

Variance properties of the microwave absorption spectrum of an ensemble of nitrogen vacancy centers in diamond

R. A. Chelly, T. Chang, I. Holzman, T. Cohen, J. Kantorovitsch and M. Stern[(a)]

Quantum Nanoelectronics Laboratory, Physics Department and Bar-Ilan Institute of Nanotechnology and Advanced Materials (BINA) - 5290002 Ramat-Gan, Israel

received 28 August 2023; accepted in final form 30 November 2023
published online 21 December 2023

Abstract – This work presents an original method based on the variance properties of the microwave absorption spectrum of an ensemble of nitrogen vacancy centers in diamond. The spectrum is measured optically. A compact and simple device is designed to optimize the photon collection. We conduct a quantitative comparison of the ensemble's optical signal in both the visible and near infrared range. Using the enhanced signal-to-noise ratio achieved through the device geometry we perform real-time DC magnetometry at moderate light and microwave powers. Under these conditions, the amplitude of a DC magnetic field can be extracted from the variance of the microwave absorption spectrum in a fast and reproducible manner, without the burden of complex fitting techniques.

Introduction. – Despite their demonstrated applications in various fields [1–5], the actual performance of nitrogen vacancy (NV) centers in diamond as magnetic sensors remains far from their theoretical limits [6,7]. Some of the limitations of these sensors are intrinsic. For instance, the NV center spin can exhibit long relaxation times at room temperatures [8] but its dephasing time is typically much shorter, especially in diamonds with high nitrogen concentration [9]. Another common limitation of NV sensors is the poor collection efficiency of the emitted photons due to the total internal reflection resulting from diamond's high refractive index. As a result, state-of-the-art NV magnetometers exhibit $\mathrm{nT}/\sqrt{\mathrm{Hz}}$ sensitivities [5,10] while other technologies such as atomic vapors on a chip [11] may have sensitivities at the $\mathrm{fT}/\sqrt{\mathrm{Hz}}$ level and below. Clearly, the main advantages of NV centers are their robustness and their possibilities in terms of spatially resolved measurements [1,12–14]. However, increasing the signal-to-noise ratio of these sensors is imperative if one wishes to detect rather weak magnetic fields with moderate power in realistic sampling times.

In the last decade, several successful approaches have been reported in the literature in order to collect more efficiently the NV fluorescence signal [15–19]. Due to total internal reflection, an objective with a numerical aperture $NA = 0.95$ will collect only $\sim 4\%$ of the total NV photoluminescence [15]. This collection efficiency can be improved by almost an order of magnitude if one can detect the photoluminescence emitted from the sides of the sample. However, such a detecting scheme often increases experimental complexity and may be problematic for certain applications. In ref. [15], four photodetectors were used to detect the fluorescence emitted by the four edges of the sample. Along these lines, several works [16,19] employed a trapezoidally cut diamond chip and a parabolic concentrator or coupling prisms to improve collection efficiency.

In this work, we present a simple and compact device capable of collecting a large amount of the photons emitted by an NV ensemble and compare the optical signal in the visible and near infrared range. We apply the enhanced signal-to-noise ratio gained from the device geometry to perform real-time DC magnetometry with moderate light power, compatible with possible future low-temperature or *in vivo* measurements. We demonstrate that the amplitude of the magnetic field can be directly extracted from the variance of the microwave absorption spectrum, without the burden of complex fitting techniques. In the following, we will show that the spectrum variance depends quadratically on the amplitude of the applied magnetic field. This measurement is extremely simple to implement and requires minimal computational resources. Moreover, this technique is relatively robust to systematic errors arising from strain, electric field or temperature variations. We believe this scheme may be useful for magnetic field navigation systems [20], which require fast, real-time scalar magnetic field measurements. Using a magnetic

[(a)]E-mail: michael.stern@biu.ac.il (corresponding author)

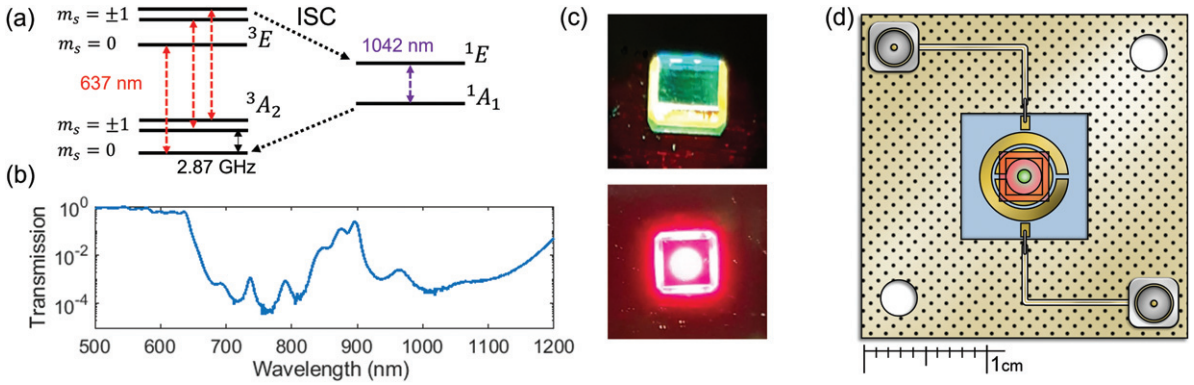

Fig. 1: (a) Level diagram of an NV center showing the ground state triplet spin $^3A_2$ and its zero-field splitting frequency $D = 2.87\,\text{GHz}$, the excited state ^3E obtained after optical excitation, as well as the singlet states ^1E and $^1A_1$ involved in the triplet-singlet intersystem crossing (ISC). (b) Transmission properties of the double band TiO_2/SiO_2 dielectric Bragg filter at zero incident angle on a microscope glass coated simultaneously with the diamond samples. (c) Top: view of the polished facets of the diamond sample covered by the dielectric Bragg filter. Bottom: view of the diamond top side showing the emitted red fluorescence from the sample and on its sides. (d) Schematical representation showing the diamond and the split ring resonator glued to a PCB. The outer radius of the SRR is $R_{out} = 3.54\,\text{mm}$, the width of the rings are $w = 1\,\text{mm}$ and the spacing between rings is set to $s = 0.2\,\text{mm}$.

field map, the variance technique could be used for correcting cumulative errors of an inertial navigation system as well as for biosensing and imaging applications using nanodiamonds.

Experimental system. – Figure 1(a) shows the energy level diagram of an NV center. The center ground state is a $^3A_2$ spin triplet. This ground state can be excited optically into an ^3E state with a zero phonon line (ZPL) at 637 nm. The states $m_s = \pm 1$ have a significantly higher probability than $m_s = 0$ to undergo a triplet-singlet intersystem crossing (ISC) from ^3E to state ^1E. An NV center which undergoes ISC then decays to another long lived singlet level $^1A_1$, after which it crosses over the $m_s = 0$ sublevel of the $^3A_2$ ground state [21]. Thus, after interaction with sufficiently intense light exciting the $^3A_2 \rightarrow ^3E$ transition, the $m_s = \pm 1$ sublevels become depopulated and up to 90% of the total population can accumulate in the $m_s = 0$ ground state [22,23]. Furthermore, NV centers with $m_s = 0$ have a higher probability for visible fluorescence than those with $m_s = \pm 1$ which can either decay non-radiatively or by emitting a near infrared fluorescence photon [21,24]. This last property enables the optical readout of the spin state by measuring the intensity of the visible or near infrared fluorescence emission.

The two samples studied in this work (see fig. 1(c)) are synthetic single crystal diamond chips grown by chemical vapor deposition (Element 6, DNV-B1 and DNV-B14). Their dimensions are $3 \times 3 \times 0.5\,\text{mm}$ and they are polished along the [1 0 0] crystallographic direction with surface roughness average $R_a < 30\,\text{nm}$. They contain substitutional nitrogen defects at a concentration of approximately 0.8 ppm for sample DNV-B1 (hereafter referred to as the "pink" diamond) and approximately 13 ppm for DNV-B14 (hereafter referred to as the "red" diamond). These concentrations are a good trade-off between large NV concentration and good coherence properties [9] assuming natural isotopic abundance of ^{13}C. After appropriate treatment, the conversion efficiency into nitrogen vacancy is relatively high, approximately 30%. To enhance the photon collection efficiency, a dielectric double band Bragg filter was deposited on the bottom side of the diamonds. The deposition of the filter was carried out using Ion Beam Sputtering (IBS) on a Nanoquest machine from INTLVAC. The filter is composed of 24 pairs of alternating TiO_2 and SiO_2 layers. The first 12 pairs have layer widths equal to a quarter of the first band's central wavelength ($\lambda = 720\,\text{nm}$), while the 12 remaining pairs have layer widths equal to a quarter of the second band's central wavelength ($\lambda = 1080\,\text{nm}$). This filter is designed to have a normal incidence reflectivity of $\sim 99\%$ in the range between 660–840 nm and 910–1170 nm while being almost transparent to green light illumination. We measured the transmission properties of a microscope glass coated simultaneously with the diamond sample and found good agreement between the theoretical and experimental curves (see fig. 1(b)).

The diamond samples are positioned at the center of a split-ring resonator (SRR) shown in fig. 1(d). The SRR comprises a pair of concentric open rings with slits on opposite sides [25]. It is fabricated on a sapphire square plate which contains a through hole at its center for illumination of the diamond. Using an electromagnetic microwave simulator (Ansys HFSS), we determined the SRR dimensions that match its resonance frequency with that of NV centers at zero magnetic field (2.87 GHz). Namely, the outer radius is $R_{out} = 3.54\,\text{mm}$, the width of the rings are $w = 1\,\text{mm}$ and the spacing between rings is set to $s = 0.2\,\text{mm}$. To fabricate the resonator, a 20 nm thin adhesion layer of titanium is first evaporated on the sapphire

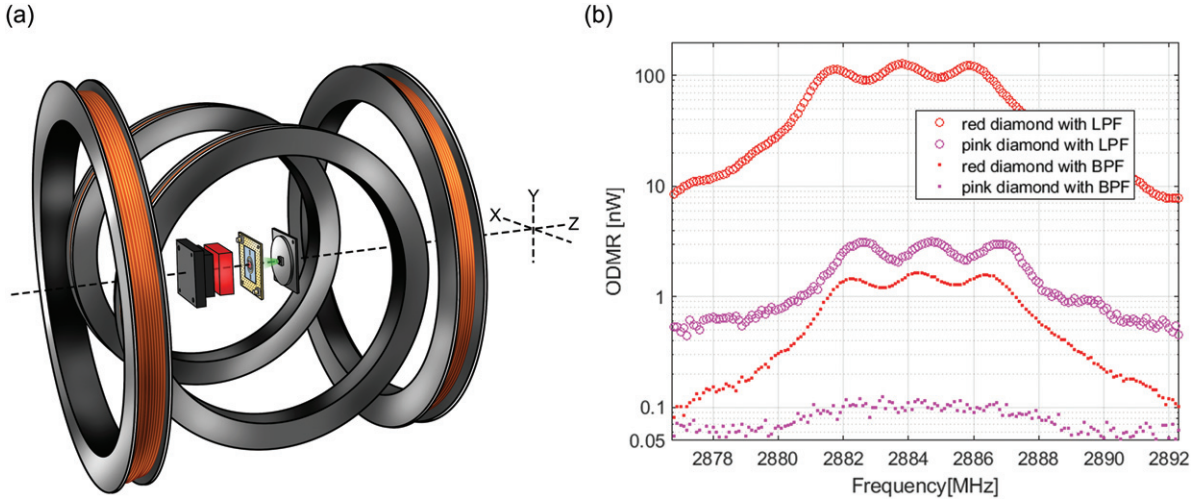

Fig. 2: (a) Three-dimensional schematic representation of the experimental setup showing the Helmoltz coils, the green LED, the split ring resonator and the diamond mounted on the PCB, a red long-pass filter and the back of a 10×10 mm silicon photodiode. (b) Optically detected magnetic resonance (ODMR) spectra for an external magnetic field of amplitude $B_z = 1$ mT applied in the Z-direction for different configurations: red diamond on red LPF (red circles), pink diamond on red LPF (pink circles), red diamond on IR BPF (red dots) and pink diamond on IR BPF (pink dots).

by e-beam evaporation followed by deposition of 300 nm of gold by magnetron sputtering. Optical resist is then spun on the sapphire plate and the resonator is patterned with UV laser lithography. After development, the sapphire plate is etched with gold etchant (KI/I2) followed by a mixture of H_2O:HF:H_2O_2 (20:1:1 volume ratio) to remove the adhesion layer and then cleaned overnight in N-methyl 2-pyrrolidone (NMP). The resonator is glued with PMMA resist on a microwave printed circuit board (PCB) made out of TMM10 ceramics and its transmission is measured with a Vector Network Analyzer. The bare resonance frequency of the SRR is $f_r^{bare} = 3.13$ GHz and its quality factor $Q = 20$. When the diamond sample is placed at the center of the resonator, the resonance frequency is slightly shifted down to $f_r^{loaded} = 2.92$ GHz in agreement with the results of our electromagnetic simulation and ref. [25].

Figure 2(a) shows a three-dimensional schematic representation of the experimental setup. The device is placed at the center of a vector magnet to apply a magnetic field in the Z- and/or X-direction. The diamond sample is illuminated at 530 nm by a light emitting diode (LED) via a hole in the PCB of diameter $d = 1.5$ mm and with uniform power density $I_L \sim 0.45\,\mathrm{W/cm^2}$. To compare the fluorescence in the visible and infrared range, the optical signal is filtered either by a long-pass red filter (LPF) with optical density OD7 at 530 nm or by a bandpass infrared (IR) filter (BPF) with OD6 for wavelengths below 960 nm. The filtered signal is then collected by a 10×10 mm silicon photodiode of responsivity $\mathcal{R} = 0.45$ A/W at 700 nm and $\mathcal{R} = 0.35$ A/W at 1040 nm and low dark current (200 pA).

By simple arguments, it is possible to show that a large part of the NV fluorescence should be collected by the photodetector. Photons emitted with an angle ζ below the full reflection angle ($\zeta_c \sim 24.5°$ for an air/diamond interface) are directly collected or reflected with the help of the bottom Bragg reflector and then collected with almost 100% efficiency. Since the absorption of the diamond is negligible in the range of the NV^- fluorescence spectrum (630–1100 nm), light emitted with an angle $\zeta > \zeta_c$ will be reflected back and forth until it reaches the sides of the sample. The sides of the sample have been polished to form prisms with an angle $\psi \sim 40°$ and are covered with a 150 nm thick aluminum layer that will totally reflect rays if $\zeta > \zeta_c$. These photons should then be collected by the photodetector with almost 100% efficiency.

In order to be more quantitative, we conducted a simulation using Optilayer, an optical coating design software. This software enables the calculation of transmission and reflection spectra at any angle of incidence for multilayer coatings, provided the refractive indices of the deposited materials are known. Additionally, it allows the computation of the reflection of a specified light cone based on a given light intensity distribution. We computed the optical transmission through the surface coated with the Bragg filter, assuming a uniform angular and spectral intensity distribution ranging from +90 to −90 degrees and wavelengths between 650 and 800 nm. The simulation resulted in a transmission value of $T_{Bragg} = 0.3\%$. In contrast, the uncoated surface exhibited a transmission value of $T_u = 7.75\%$ under the same angular and spectral intensity distribution. Assuming no optical absorption in the diamond and neglecting losses from the side of the diamond, we determined that the collection efficiency of NV fluorescence amounts to $T_u/(T_u + T_{Bragg}) = 96.3\%$. It is important to note that this value represents a theoretical upper bound, as the reflectivity of the aluminum layer coated on the side of the sample is not 100% and the loss in the diamond is not zero.

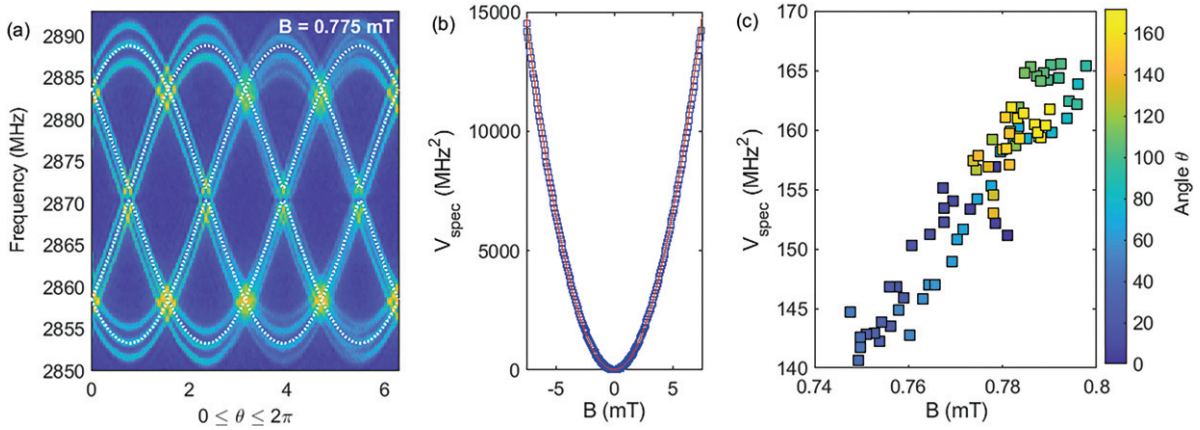

Fig. 3: (a) ODMR spectra at almost constant magnetic field ($B \sim 0.775\,\mathrm{mT}$) *vs.* magnetic field angle θ rotating in the (X, Z)-plane (represented in fig. 2(a)). The dotted white lines correspond to approximated solutions of the Hamiltonian of the system according to eq. (1). (b) Spectrum variance V_{spec} *vs.* magnetic field applied in the Z-direction. The red line corresponds to fitting curve $\alpha^2 B^2 + \beta^2$ with $\alpha = 16.18\,\mathrm{GHz/T} (\simeq \gamma/\sqrt{3})$ and $\beta = 2.15\,\mathrm{MHz}$. (c) Spectrum variance V_{spec} of the ODMR spectra shown in (a) *vs.* slight changes of the amplitude of the rotating magnetic field oriented with different angles $\theta \in [0, \pi]$ in the (X, Z)-plane. For this measurement, we used the pink diamond. The signal to noise ratio $\eta = 30$ and the relative error on the variance $\delta V_{spec}/V_{spec}$ was approximately 0.5%.

According to ref. [26], the optical absorption cross-section of NV centers at 532 nm is $\sigma_{532} \simeq 3 \times 10^{-17}\,\mathrm{cm}^2$ and their quantum efficiency $\sim$ 50%. Thus, the optical absorption of the pink diamond with a NV density of 0.3 ppm should be $\sim$ 8%. Taking into account the reflection of the incident light at 532 nm ($\sim$ 15%), we would expect a total emitted fluorescence of 0.27 mW. The DC current detected by the photodiode when using the pink diamond on LPF is $I_{DC} = 86\,\mu\mathrm{A}$ corresponding to 0.2 mW of collected light, which is very close to what is expected from this rough estimate. In the following, this DC photocurrent is compensated by an external offset so the AC components of the signal can be converted to voltage by a transimpedance amplifier of gain $\mathcal{G} = 80\,\mathrm{kV/A}$ and input current noise density $0.8\,\mathrm{pA}/\sqrt{\mathrm{Hz}}$.

Microwave absorption spectrum of the NV ensemble. – The microwave absorption spectrum of the NV ensemble is detected optically. When the frequency of a microwave drive inserted in the SRR is in resonance with one of the $m_s = 0$ to $m_s = \pm 1$ transitions of the $^3A_2$ ground state triplet, the fluorescence of the NV ensemble is slightly modified (see fig. 1(a)). In order to detect this change, we use a digital step attenuator to modulate the amplitude of the microwave signal at $f_{mod} = 127\,\mathrm{Hz}$. The photocurrent thus contains an AC component directly proportional to the microwave absorption. This signal is demodulated via a lock-in amplifier and can be recorded in real time by a Field Programmable Gate Array (FPGA).

We begin our experiments by applying a magnetic field in the Z-direction. In a single diamond crystal, nitrogen vacancy centers can be oriented in four crystallographic different directions $\mathbf{u}_1 = \frac{1}{\sqrt{3}}(1,1,1)$, $\mathbf{u}_2 = \frac{1}{\sqrt{3}}(1,-1,-1)$, $\mathbf{u}_3 = \frac{1}{\sqrt{3}}(-1,1,-1)$ or $\mathbf{u}_4 = \frac{1}{\sqrt{3}}(-1,-1,1)$ and are randomly and uniformly distributed over them. A bias field in the Z-direction projects equally all four orientations and thus the spin resonances overlap. At $B_z = 1\,\mathrm{mT}$, the spectrum consists of six Lorentzian peaks forming two well-distinguished triplets. The distance between the two triplets is 32.55 MHz and corresponds to the expected Zeeman splitting $2\gamma B/\sqrt{3}$ where $\gamma = 28.02\,\mathrm{GHz/T}$ is electron spin gyromagnetic ratio. The peaks of the triplets are separated by a constant splitting $A = 2.16\,\mathrm{MHz}$. This splitting is due to hyperfine coupling with ^{14}N nuclei present in each NV center.

Figure 2(b) shows one of the two triplets measured using different setups under the same experimental conditions ($B_z = 1\,\mathrm{mT}, I_L = 0.45\,\mathrm{W/cm}^2, P_{mw} = 15\,\mathrm{dBm}$). The lock-in time constant was fixed at 10 ms and its equivalent noise bandwidth (ENBW) was $\Delta f = 7.8\,\mathrm{Hz}$ per spectrum data point for all measurements. The red diamond fluorescence was found to be approximately 30–40 times larger than the pink diamond signal, both in the visible and infrared range. This ratio is directly proportional to the concentration ratio of NV centers in the two samples. The amplitude of the near infrared fluorescence signal is smaller by two orders of magnitude than in the visible range due to competition with other non-radiative processes [21]. The signal to noise ratio is limited by current shot noise, except for the infrared measurement of the pink diamond where shot noise becomes comparable to the noise generated by the transimpedance amplifier.

The microwave absorption spectrum is more complex if the field is applied in an arbitrary direction. To illustrate this point, we represent in fig. 3(a) the spectra when rotating the magnetic field for constant field amplitude $B \sim 0.8\,\mathrm{mT}$. The angle θ is the angle between the Z-axis (shown in fig. 2(a)) and the direction of the rotating magnetic field, which stays in the (X,Z)-plane

as represented in fig. 2(a). The magnitude of the signal is color-coded with yellow color indicating strong absorption. The signal to noise ratio of this measurement was $\eta = 30$. We represent with dotted white lines approximated solutions of the Hamiltonian (see the Supplementary Material `Supplementarymaterial.pdf` (SM)) which behave according to the following equation:

$$\nu_{\pm} = D \pm \sqrt{\gamma^2 B_{\parallel}^2 + E^2} + \frac{3\gamma^2 B_{\perp}^2}{2D}, \tag{1}$$

where $D = 2.87\,\mathrm{GHz}$ is the axial zero-field splitting, $E \simeq 800\,\mathrm{kHz}$ is the off-axis zero-field splitting resulting from local strain in the diamond, $B_{\parallel}$ is the value of the projection of the magnetic field along the NV axis and $B_{\perp}$ its transverse component.

Using microwave absorption spectrum to extract the components of an arbitrary magnetic field is relatively simple and straightforward if one can measure independently several single NV centers with different well-known quantization directions [14]. For an ensemble of NV centers with randomly distributed axis directions, an additionnal information is needed. This information can be provided for instance by the application of a reference magnetic field [5] or by the amplitude of photoluminescence, which varies when the quantization axis changes. Usually, the magnetometer measures the field by sweeping the frequency accross the full microwave absorption spectrum [27,28]. In this case, the precision of the field measurement δB is directly related to the precision of the peak positions which can be extracted by a fit procedure. The uncertainty of the fit procedure is given by $\sqrt{\Gamma d}/\eta$ [29] where Γ is the width of the Lorentzian peaks, η is the signal to noise ratio and d is the frequency separation between adjacent data points. Thus, $\delta B \sim \sqrt{3\Gamma d}/(2\gamma\eta)$. With the parameters of our system in the best configuration ($\Gamma = 1.94\,\mathrm{MHz}$, $d = 100\,\mathrm{kHz}, \eta = 170$, red diamond with red LPF), we obtain a precision $\delta B = 80\,\mathrm{nT}$.

Variance properties. – In the following, we demonstrate an interesting property of the variance of the microwave absorption spectrum. This property can be used to easily extract the amplitude of an external magnetic field applied in an arbitrary direction without acquiring the full spectra and fitting with the Hamiltonian of the system. Let us therefore consider an arbitrary magnetic field of amplitude B and direction $\mathbf{u}$. We introduce the variance $\mathscr{V}$ defined as

$$\mathscr{V} = \frac{1}{8}\sum_{i=1}^{4}(\nu_{\pm}^{i} - D)^2. \tag{2}$$

Using eq. (1) with $B_{\parallel}^{i} = B(\mathbf{u}\cdot\mathbf{u}_i)$ and the relation $\sum_{i=1}^{4}(\mathbf{u}\cdot\mathbf{u}_i)^2 = \frac{4}{3}$ it is possible to show that

$$\mathscr{V} \simeq \frac{\gamma^2 B^2}{3} + E^2. \tag{3}$$

A detailed calculation is given in the SM. In particular, it is possible to show that the error goes like $O(\frac{\gamma^2 B^2}{D^2})$ and is less than 1% for magnetic field amplitudes up to 10 mT. Taking into account the hyperfine coupling adds a constant term $2A^2/3$ which does not modify considerably the result. Thus, measuring the variance of the transition frequencies gives direct access to the amplitude of the external magnetic field. It is possible to simplify even further this analysis by introducing a slightly different definition of the variance of a microwave absorption spectrum, namely

$$V_{spec} = \frac{\sum_{j=1}^{N} R_j (f_j - \bar{f})^2}{\sum_{j=1}^{N} R_j}, \tag{4}$$

with $\bar{f} = \frac{\sum_{j=1}^{N} R_j f_j}{\sum_{j=1}^{N} R_j}$ and where the optical signal R_j has been sampled over N frequencies f_j. The spectrum variance V_{spec} is also a quadratic function of the magnetic field amplitude: $V_{spec} \simeq \alpha^2 B^2 + \beta^2$ with α and β being two constant parameters. This result is due to interesting mathematical properties of non-central moments of Gaussian distributions. If the peaks were Gaussian, the contribution to the variance of the spectrum from each resonance peak would be given by $\Gamma^2 + (\nu_{\pm}^{i} - D)^2$. Thus, the spectrum variance V_{spec} has the same behavior as $\mathscr{V}$.

This property is true to a good approximation if the peaks are nearly Gaussian. It happens that the Lorentzian shape of the peaks of an ensemble of NV centers is sufficiently close to Gaussian behavior. The advantage of such an analysis is of course its simplicity in terms of implementation in real-time systems with limited computational resources. Moreover, the total acquisition time of the spectrum can be considerably reduced if one truncates the noisy data baseline and measures only in the vicinity of the peaks. This mathematical treatment of the data has been done in fig. 3(b) and gives a nice parabolic behavior *vs.* magnetic field. We find a good match with theoretical values $\alpha = 16.2\,\mathrm{GHz/T} (\simeq \gamma/\sqrt{3})$ and $\beta = 2.15\,\mathrm{MHz}$ $(\simeq \sqrt{E^2 + \Gamma^2 + 2A^2/3})$.

In fig. 3(c), we represent the spectrum variance V_{spec} *vs.* magnetic fields applied in the (X,Z)-plane along different values of angle θ. To perform this experiment, we rotate the magnetic field in the (X,Z)-plane using a vector magnet controlled by two independent source measurement units (see fig. 2(a)). The field amplitude is kept approximately constant around $B \sim 0.8\,\mathrm{mT}$. Yet, due to small imperfections of the vector magnet, the actual amplitude of the field varies slightly and thus V_{spec} is not a constant. For each spectrum, the exact value of the applied magnetic field is extracted by fitting the full microwave absorption spectra and plotted *vs.* V_{spec}. In order to demonstrate that V_{spec} and θ are uncorrelated, we estimate the relative covariance $\mathscr{C}$ defined as

$$\mathscr{C} = \frac{\mathrm{cov}\,\left(\mathrm{V}_{spec} - \alpha^2\mathrm{B}^2, \theta\right)}{\sqrt{\mathrm{var}\,(\mathrm{V}_{spec} - \alpha^2\mathrm{B}^2) \times \mathrm{var}\,(\theta)}}. \tag{5}$$

We find that $\mathscr{C} \sim 0.07$ indicating that V_{spec} and θ are indeed well uncorrelated as expected.

We repeat the variance measurement over time for a constant field of $\sim 1\,\mathrm{mT}$ in order to verify the reproducibility and precision of our method and compare it with more conventional techniques. The average value of the variance measurement is $V_{spec} = 222.6\,\mathrm{MHz}^2$ and its standard deviation is $\delta V_{spec} = 0.018\,\mathrm{MHz}^2$. This is translated into a magnetic field precision of $\delta B = 40\,\mathrm{nT}$. Each measurement was performed in 16 s and thus the magnetic field sensitivity is $\sim 0.16\,\mu\mathrm{T}/\sqrt{\mathrm{Hz}}$.

The method of measuring the variance is relatively robust to shifts of the spectral lines. To illustrate our point, we conducted a series of experiments where we varied the temperature of the sample in a range of $+/-10$ degrees around room temperature. When we vary the temperature, the resonance peak positions shift to lower frequencies by around 80 kHz/K. This shift results in inaccuracy of the magnetic field extracted from a fit of the peak position of approximately $3\,\mu\mathrm{T/K}$. On the other hand, the variance measurement varies by less than $1\,\mathrm{MHz}^2$ over a range of 10 K. Using eq. (2), we thus obtain an inaccuracy $\delta B = B \times \delta V/(2V)$ of around $0.2\,\mu\mathrm{T/K}$ at $B = 1\,\mathrm{mT}$.

Discussion and conclusion. – In conclusion, we demonstrated that the amplitude of the magnetic field can be directly extracted from the variance of the microwave absorption spectrum. Using this method, we reached a moderate magnetic sensitivity of $0.16\,\mu\mathrm{T}/\sqrt{\mathrm{Hz}}$ with low illumination and microwave power. As a matter of comparison, ref. [5] reports a much better level of sensitivity ($\sim 50\,\mathrm{pT}/\sqrt{\mathrm{Hz}}$) and this discrepancy requires here a full explanation. The signal to noise ratio η which governs the sensitivity of the measurement is limited in both cases by shot noise. However, the amount of optical power on the sample is three orders of magnitude larger in [5]: the LED in our system provides a total illumination of 8 mW on the sample to be compared to 4.3 W of laser illumination. Additionally, the microwave power we used to drive the spins is approximately two orders of magnitude smaller than in ref. [5].

The main advantages of the variance technique is clearly its simplicity in terms of implementation and computational resources. Moreover, this technique is robust to errors coming from strain, electric field or temperature variations. The precision of the measurement can be further enhanced by using pulsed type measurement techniques such as pulsed ODMR [30]. It would be also interesting to further explore the contrast of infrared emission under red excitation. In conclusion, we believe the detection scheme developed in this work could be beneficial in several applications requiring fast real-time scalar magnetic field measurements with moderate sensitivity and power consumption.

* * *

We thank E. Buks for fruitful discussions, D. Doek for polishing the diamond sides, M. Feldberg and T. Sharabi for sputtering the metal used in our SRR, Y. Elbaz for design on solidworks, and M. Oksman for his technical support. This research was supported by the Israeli Science Foundation under grant Nos. 898/19 and 963/19.

Data availability statement: All data that support the findings of this study are included within the article (and any supplementary files).

REFERENCES

[1] Pham L. M., Sage D. L., Stanwix P. L., Yeung T. K., Glenn D., Trifonov A., Cappellaro P., Hemmer P. R., Lukin M. D., Park H., Yacoby A. and Walsworth R. L., *New J. Phys.*, **13** (2011) 045021.
[2] Schirhagl R., Chang K., Loretz M. and Degen C. L., *Annu. Rev. Phys. Chem.*, **65** (2014) 83.
[3] Barry J. F., Turner M. J., Schloss J. M., Glenn D. R., Song Y., Lukin M. D., Park H. and Walsworth R. L., *Proc. Natl. Acad. Sci. U.S.A.*, **113** (2016) 14133.
[4] Glenn D. R., Fu R. R., Kehayias P., Sage D. L., Lima E. A., Weiss B. P. and Walsworth R. L., *Geochem. Geophys. Geosyst.*, **18** (2017) 3254.
[5] Schloss J. M., Barry J. F., Turner M. J. and Walsworth R. L., *Phys. Rev. Appl.*, **10** (2018) 034044.
[6] Budker D. and Romalis M., *Nat. Phys.*, **3** (2007) 227.
[7] Barry J. F., Schloss J. M., Bauch E., Turner M. J., Hart C. A., Pham L. M. and Walsworth R. L., *Rev. Mod. Phys.*, **92** (2020) 015004.
[8] Jarmola A., Acosta V. M., Jensen K., Chemerisov S. and Budker D., *Phys. Rev. Lett.*, **108** (2012) 197601.
[9] Bauch E., Singh S., Lee J., Hart C. A., Schloss J. M., Turner M. J., Barry J. F., Pham L. M., Bar-Gill N., Yelin S. F. and Walsworth R. L., *Phys. Rev. B*, **102** (2020) 134210.
[10] Acosta V. M., Bauch E., Jarmola A., Zipp L. J., Ledbetter M. P. and Budker D., *Appl. Phys. Lett.*, **97** (2010) 174104.
[11] Kitching J., *Appl. Phys. Rev.*, **5** (2018) 031302.
[12] Taylor J. M., Cappellaro P., Childress L., Jiang L., Budker D., Hemmer P. R., Yacoby A., Walsworth R. and Lukin M. D., *Nat. Phys.*, **4** (2008) 810.
[13] Maertz B. J., Wijnheijmer A. P., Fuchs G. D., Nowakowski M. E. and Awschalom D. D., *Appl. Phys. Lett.*, **96** (2010) 092504.
[14] Wang P., Yuan Z., Huang P., Rong X., Wang M., Xu X., Duan C., Ju C., Shi F. and Du J., *Nat. Commun.*, **6** (2015) 6631.
[15] Le Sage D., Pham L. M., Bar-Gill N., Belthangady C., Lukin M. D., Yacoby A. and Walsworth R. L., *Phys. Rev. B*, **85** (2012) 121202.
[16] Wolf T., Neumann P., Nakamura K., Sumiya H., Ohshima T., Isoya J. and Wrachtrup J., *Phys. Rev. X*, **5** (2015) 041001.
[17] Clevenson H., Trusheim M. E., Teale C., Schröder T., Braje D. and Englund D., *Nat. Phys.*, **11** (2015) 393.
[18] Riedel D., Söllner I., Shields B. J., Starosielec S., Appel P., Neu E., Maletinsky P. and Warburton R. J., *Phys. Rev. X*, **7** (2017) 031040.

[19] Ma Z., Zhang S., Fu Y., Yuan H., Shi Y., Gao J., Qin L., Tang J., Liu J. and Li Y., *Opt. Express*, **26** (2018) 382.
[20] Clevenson H., Pham L. M., Teale C., Johnson K., Englund D. and Braje D., *Appl. Phys. Lett.*, **112** (2018) 252406.
[21] Acosta V. M., Jarmola A., Bauch E. and Budker D., *Phys. Rev. B*, **82** (2010) 201202.
[22] Felton S., Edmonds A. M., Newton M. E., Martineau P. M., Fisher D., Twitchen D. J. and Baker J. M., *Phys. Rev. B*, **79** (2009) 075203.
[23] Grezes C., Julsgaard B., Kubo Y., Stern M., Umeda T., Isoya J., Sumiya H., Abe H., Onoda S., Ohshima T., Jacques V., Esteve J., Vion D., Esteve D., Mølmer K. and Bertet P., *Phys. Rev. X*, **4** (2014) 021049.
[24] Rogers L. J., Armstrong S., Sellars M. J. and Manson N. B., *New J. Phys.*, **10** (2008) 103024.
[25] Bayat K., Choy J., Farrokh Baroughi M., Meesala S. and Loncar M., *Nano Lett.*, **14** (2014) 1208.
[26] Fraczek E., Savitski V. G., Dale M., Breeze B. G., Diggle P., Markham M., Bennett A., Dhillon H., Newton M. E. and Kemp A. J., *Opt. Mater. Express*, **7** (2017) 2571.
[27] Steinert S., Dolde F., Neumann P., Aird A., Naydenov B., Balasubramanian G., Jelezko F. and Wrachtrup J., *Rev. Sci. Instrum.*, **81** (2010) 043705.
[28] Nowodzinski A., Chipaux M., Toraille L., Jacques V., Roch J.-F. and Debuisschert T., *Microelectron. Reliab.*, **55** (2015) 1549.
[29] Jupp P., Harris K. and Aliev A., *J. Magn. Reson.*, **135** (1998) 23.
[30] Dréau A., Lesik M., Rondin L., Spinicelli P., Arcizet O., Roch J.-F. and Jacques V., *Phys. Rev. B*, **84** (2011) 195204.